POLITECNICO DI TORINO
Repository ISTITUZIONALE

A Force Control Test Rig for the Dynamic Characterization of Helicopter Primary Flight Control Systems

Original
A Force Control Test Rig for the Dynamic Characterization of Helicopter Primary Flight Control Systems / Bertucci, A., Mornacchi, A., Jacazio, G., Sorli, M.. - In: PROCEDIA ENGINEERING. - ISSN 1877-7058. - 106:(2015), pp. 71-82. [10.1016/j.proeng.2015.06.010]

Availability:
This version is available at: 11583/2648425 since: 2016-09-13T09:07:44Z

Publisher:
Elsevier Ltd

Published
DOI:10.1016/j.proeng.2015.06.010

Terms of use:

This article is made available under terms and conditions as specified in the corresponding bibliographic description in the repository

Publisher copyright

(Article begins on next page)

15 October 2026

Available online at www.sciencedirect.com

ScienceDirect

Procedia Engineering 106 (2015) 71 – 82

Procedia Engineering

www.elsevier.com/locate/procedia

Dynamics and Vibroacoustics of Machines (DVM2014)

A force control test rig for the dynamic characterization of helicopter primary flight control systems

Alessandro Bertucci*, Andrea Mornacchi, Giovanni Jacazio, Massimo Sorli

Politecnico di Torino, Corso Duca degli Abruzzi 24, Torino, 10129, Italy

Abstract

This paper describes an electronically controlled active force control system developed to test the tail rotor actuator of a new medium size helicopter. As for all hydraulic force control systems, the critical control issue is to mitigate the disturbance generated by the actuator velocity. For this particular case, the problem was accrued by the high bandwidth of the tail rotor actuator. To define the optimum control algorithm a model based approach was followed, estimating, when unable to measure directly, mechanical and hydraulic model parameters with a dedicated experimental campaign. A controller was eventually developed able to cope with the severe dynamic disturbances by introducing velocity and acceleration compensation laws. The controller was then implemented in a high recursion rate real time machine interfacing with a servovalve controlling the flow to a hydraulic actuator provided with hydrostatic bearings to minimize the friction force. The actuator force was sensed by a load cell providing the feedback signal for the force servoloop. A critical feature of the control was the need to develop a dedicated complex filter for the velocity signal able to cancel out the signal noise while allowing to retain the correct real time information of the actuator velocity and maintain adequate stability margins.

© 2015 Published by Elsevier Ltd. This is an open access article under the CC BY-NC-ND license (http://creativecommons.org/licenses/by-nc-nd/4.0/).

Peer-review under responsibility of organizing committee of the Dynamics and Vibroacoustics of Machines (DVM2014)

Keywords: *Force control; hydraulic servosystem; helicopter primary flight controls; disturb rejection; linear analysis; static characteristic*

* Corresponding author. Tel.: +39 011 090 6942
E-mail address: alessandro.bertucci@polito.it

1877-7058 © 2015 Published by Elsevier Ltd. This is an open access article under the CC BY-NC-ND license (http://creativecommons.org/licenses/by-nc-nd/4.0/).

Peer-review under responsibility of organizing committee of the Dynamics and Vibroacoustics of Machines (DVM2014)
doi:10.1016/j.proeng.2015.06.010

1. Introduction

The tail rotor actuator (TRA) is an equipment utilized in rotor wing aircraft to change the collective pitch of the tail rotor to counteract the torque generated by the main rotor and to permit yaw control in response to the pilot commands. In synthesis the TRA is a position controlled hydraulic servosystem accepting the pilot command (xin) at one end of an input lever and the position feedback (xout) at the opposite end of the same lever, which performs the algebraic sum of command and feedback, thereby closing the position servoloop. An intermediate point of the input lever thus travels of an amount proportional to the difference between (xin) and (xout) and drives a linkage mechanism which eventually moves the spool of a valve controlling the flow to the hydraulic actuator. The TRA is a stiff and compact assembly designed for minimum mass and envelope.

Fig. 1. Tail Rotor Actuator

The airframe manufacturer specifies the required actuator performances, for example: rated and stall loads magnitude, waveform type, stroke, rated speed and bandwidth of the position servoloop. For TRA in analysis the most demanding condition in the load spectrum specified, design drivers in the definition of the test rig equipment, was a high frequency (100 Hz) harmonic load with variable mean value between load layers.

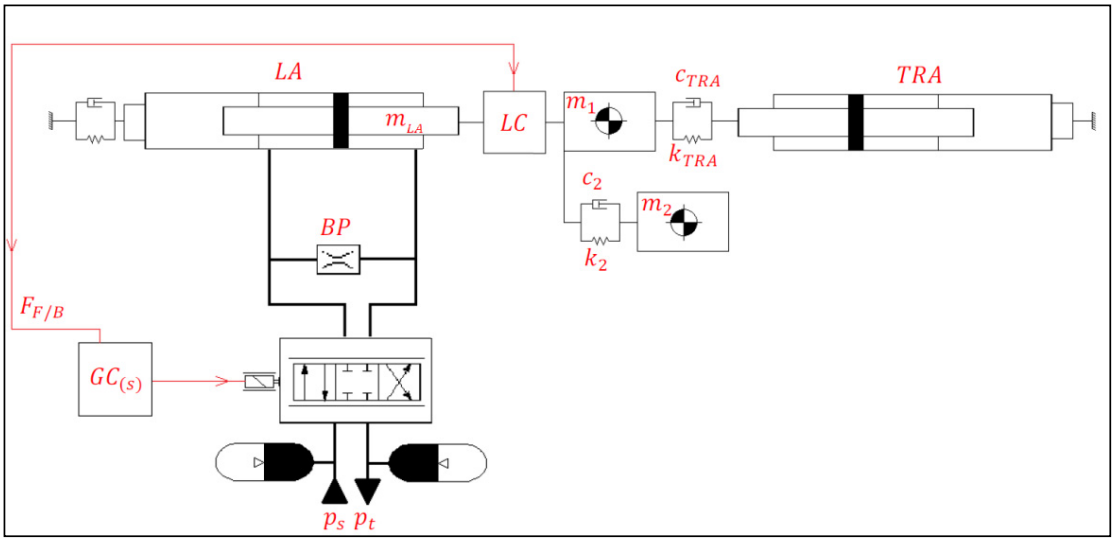

Fig. 2. Functional diagram of the force control test rig

Nomenclature

x_{LA}	Load actuator cylinder linear displacement
k_{TRA}	Tail rotor actuator stiffness
k_2	Spring constant of the fixture between mass 1 and 2
c_{LA}	Load actuator damping coefficient
c_{TRA}	Tail rotor actuator damping coefficient
c_2	Damping constant of the fixture between mass 1 and 2
m_{LA}	Mass of the load actuator rod
m_1	Mass of the first airframe inertia simulator
m_2	Mass of the second airframe inertia simulator
Q_A	Flow through the servovalve
K_{SV}	Servovalve static gain
X_{com}, V	Servovalve command signal
p_s	Supply pressure
p_t	Return pressure
Δp_l	Differential pressure between the load actuator chambers
K_o	Orifice flow gain
p_{c1}	Pressure in the chamber 1 of the load actuator
p_{c2}	Pressure in the chamber 2 of the load actuator
F	Force set
F_C	Force feedback
$\hat{F}_C$	Peak value of the force feedback
F_D	Force induced by kinematic disturbs
f_F	Frequency of the load set
K_1,K_2	Group coefficient
s	Laplace variable
τ	Time constant of the hydraulic load system
A	Piston area of the load actuator
k_L	Linearized leakage coefficient
C	Load actuator chamber capacity
G_Q	Servovalve flow gain
G_P	Servovalve pressure gain
m	Global translating mass
σ_V	Natural pulsation of the servovalve
σ_R	Natural pulsation of the load cell
K_P, K_I, K_D	Proportional, integral and derivative controller gains
G	Goodness of model fitting
F_{Ci}	i-th feedback force value acquired
F_{SIMi}	i-th simulated force value
FF_V	Feedforward coefficient for speed compensation
FF_A	Feedforward coefficient for acceleration compensation
n	Length of the acquired/simulated force vector

2. Force control test rig

In order to evaluate the TRA performance under the operating load a hydraulic force control test rig has been designed and built applying the knowledge gained during the programs which led to the publications [1], [2] and [3]. The test rig concept diagram is shown in figure 2 and a picture of the bench is presented below in figure 3.

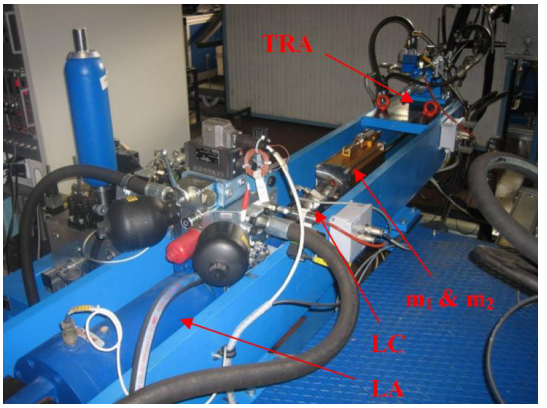

Fig. 3. View of the test rig

The TRA and the loading actuator (LA) are mounted with the cylinders rods in opposition, with a load cell and a carriage containing two linked masses placed in between. The carriage is fixed to the TRA in order to replicate the inertial properties of the tail rotor and reproduce the inertial loads due to the TRA movements. The loading actuator is mounted to the rig frame via a plate having a precise stiffness to replicate the helicopter's airframe behavior under load.

The load actuator is a hydrostatically supported balanced area cylinder. The hydrostatic supports guarantee a very small static friction (about 50 N) while the balanced area construction allows a symmetrical behavior for compression and traction load commands. A maximum load of about 50 kN can be developed by the LA providing it with full authority over the TRA which can thus be stalled.

A hydraulic manifold is directly mounted on the LA structure and its mainly comprised of two hydropneumatic bladder accumulators, on the supply and return ports, attenuating the pressures variation caused by the rig operation, a flow control servovalve, with dedicated external electronics closing the spool position loop, and a fixed diameter bypass orifice placed across the two control ports. The use of a single flow control valve instead of two pressure regulating valves is mainly due to the bandwidth requirement for the load control system which was 100 Hz.

The most important physical parameters of the rig are monitored by high bandwidth sensors which provide signals proportional to LA force (load cell), TRA displacement (LVDT) and LA piston velocity (LVT). Since the instruments providing critical feedback data are upmarket equipment, it has been possible to neglect their internal dynamics in the control design and implementation phase. The sensors signals are acquired by a real time digital controller (PXI-8108), equipped with an I/O board (PXI-6259), capable of a recursion rate of 4 kHz for the force control loop.

3. Static characteristics of the force control system

Assuming fixed the rod end of the loading actuator, neglecting the cross-chamber leakage in the LA and disregarding the dynamic behavior of all the components the steady-state performance of the force control system can be easily determined from the well-known pressure-flow relationships for a servovalve and a bypass orifice.

With reference to the hydraulic diagram of figure 4, the following equations apply:

$$Q_A = K_{SV}\, x_{com} \sqrt{p_s - p_t - \Delta p_l \cdot sign(x_{com})} \tag{1}$$

$$Q_o = K_o sign(\Delta p_l)\sqrt{|\Delta p_l|} \quad (2)$$

$$\Delta p_l = p_{c1} - p_{c2} \quad (3)$$

where:

Q_A and Q_o are the flows through the servovalve and the orifice; K_{SV} and K_o are the flow gain of the servovalve and the orifice; p_s, p_t, p_{c1} and p_{c2} are, respectively, the supply pressure, the return pressure and the pressures in the cylinder's chambers 1 and 2; x_{com} represent the normalized servovalve command.

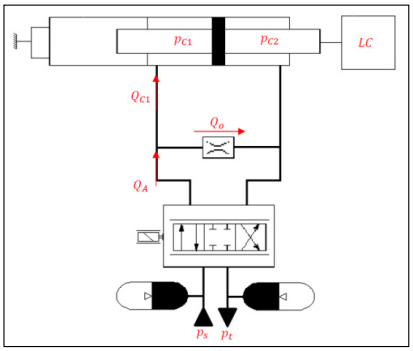

Fig. 4. Hydraulic diagram for static characteristic

In a steady state condition the flow Q_{c1} toward the chamber 1 of the load actuator is nil, thus all the servovalve flow is passing through the bypass orifice. Therefore, by setting Q_A equal to Q_o, the value of the differential pressure Δp_l across the loading actuator and hence the load actuator force can be derived as a function of the servovalve command x_{com} and of the bypass orifice and servovalve flow coefficients K_0 and K_{SV}.

The steady-state characteristic of the force control system is then obtained and is plotted in figure 5. The left diagram shows the servovalve command plotted versus the actuator force and the bypass flow for different values of the bypass orifice flow coefficient K_0. The right diagram of the same figure shows the force gain (the derivative of the actuator force versus the servovalve command) as a function of the servovalve command and for different values of the bypass orifice flow coefficient K_0. These diagrams are a helpful guide for the engineers in sizing the bypass orifice which plays a major role in the force control system behavior. Increasing the size of the bypass orifice brings about increased system damping, lower dynamic response and increased flow consumption.

A force control system without bypass orifice would be highly responsive and require minimum flow, but would be marginally stable and present low damped force oscillations. These notions coupled with the linear analysis of the force control provide the tools to perform the tradeoff study between system stability, applicable force and power requirement for the rig. A suitable control law was developed which allows the force control system to perform well with a very fast dynamic response while minimizing the size of the bypass orifice and hence the flow consumption.

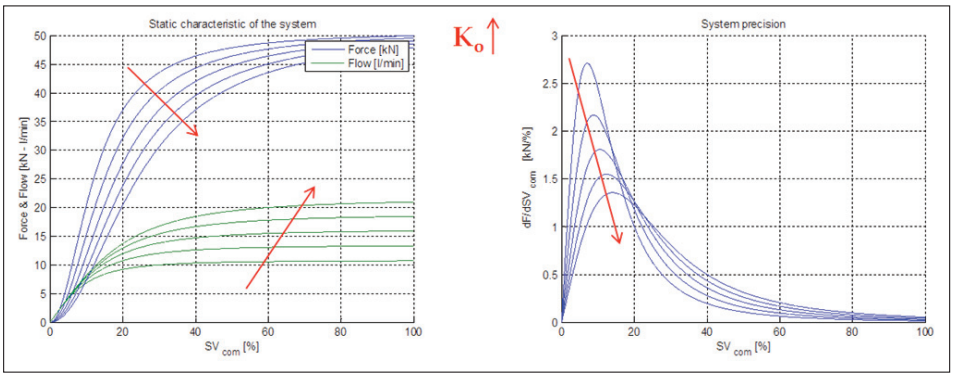

Fig. 5. Static characteristic of the force control and system accuracy

4. System modeling and simulation results

In order to develop and optimize the control law of the LA, a "physical based" mathematical model of test bench has been implemented also including the main non-linearities of the system. To this purpose a very accurate model of the servovalve was prepared. The first stage dynamic is described by a second order transfer function that includes the model of flapper end-of-travel. The equations of servovalve first stage are used to determine the second stage spool velocity and hence its position. Travel limits for the spool were also taken in due account. Once the spool position is known, the servovalve model allows the computation of the flow through each of the four internal passageways taking into account: valve laps, radial clearance between spool and sleeve and also the variation of flow discharge coefficient with the Reynolds number [4], [5].

While developing the mathematical model, special attention was given to the characteristics of the hydraulic fluid, which plays a major role in the force control system performance. Dedicated tests were carried out to precisely determine the quantity of free air in the fluid as a function of temperature, which greatly improved the confidence in the accuracy of the system simulations. Since all the equipment was directly available and provided with detailed documentation the parameters composing the model were measured, for example the static and dynamic stiffness of the TRA, or estimated indirectly either using the equations describing the physical phenomenon or imposing the convergence of the output of submodels excited by known input over a logged output.

The validation of the mathematical model was performed by comparing simulation and experimental results over a wide range of operating conditions. In order to obtain an objective evaluation of the model accuracy, a parameter G was defined which is a function of a dimensionless root mean square error for a given time history of force command [6]. The confidence parameter G is equal to 100 for a perfect match between model and experiments.

$$G = 100\left(1 - \sqrt{\frac{\sum_{i=1}^{n}\left(\frac{F_{C_i} - F_{SIM_i}}{\hat{F}_C}\right)^2}{n}}\right) \tag{4}$$

Two diagrams for two different conditions are reported hereunder with the intent that prove the quality of the mathematical model.

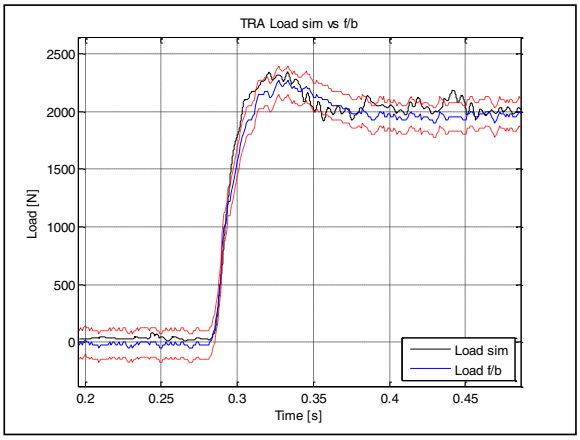

Fig. 6. Step response model validation

Figure 6 shows the experimental and simulated response for a 2 kN step command without noise on the servoactuator position. The dashed lines represent the confidence bounds of the load cell. It is possible to see the excellent fitting of the model results with the experimental data, which is confirmed by the value of the confidence parameter G = 94.95%.

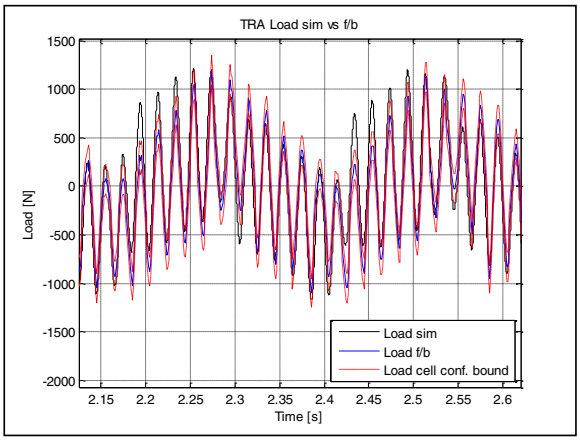

Fig. 7. Sinusoidal force set with kinematic disturbances

Figure 7 compares simulated and experimental responses to a force command 2 kN amplitude and 50 Hz frequency in presence of a TRA sine position displacement at 4 Hz frequency and 2 mm amplitude. Observing the figure it can be noted that the model overestimates the force applied to the component in specific sections of the plot, this inaccuracy is mainly due to the difficulties of synchronization of the simulated speed of the TRA to the recorded speed by which the command signal to the servovalve is calculated. This timing error results are most prominent at zero speed but after a sufficient time the hydraulic transient vanishes and the simulated force returns into the load cell confidence bounds. Also in this case the model follows well the experimental data, with a value of the confidence parameter G equal to 89.00%.

5. Force control linear analysis

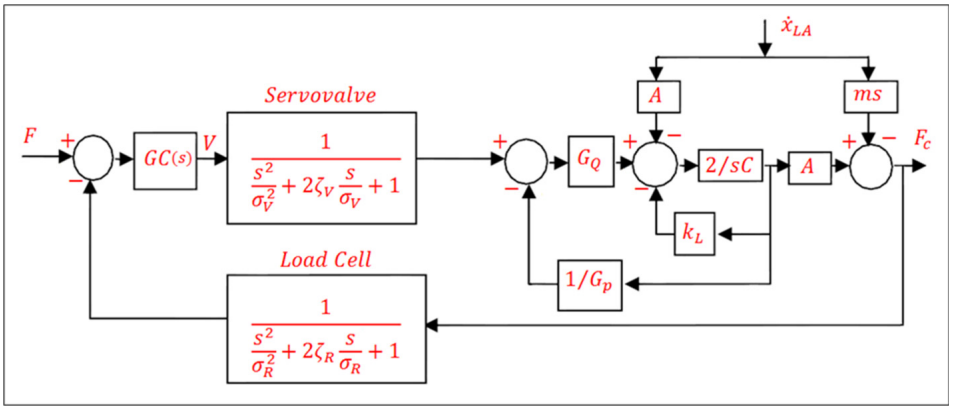

Fig. 8. Linearized force control system block diagram

Force control servosystems can use different technologies, depending on the required performance. In general, regardless of the technology [1], [2], [7], when force must be controlled on a quasi-stationary component, the parameters mostly affecting the system accuracy are the load sensor accuracy and the load actuator friction, while the component dynamics plays a minor role. However, when the load actuator must control the force on a fast moving component, such as the case of a TRA, the stiffness, damping and inertia of the system become a major source of error for the force control. The most severe disturbances on the controlled system come from the TRA velocity, which if not properly compensated by dumping the necessary amount of fluid from the loading actuator chamber whose volume is being reduced, generates an uncontrolled force spike due to the high stiffness of the load actuator. The position offset of the TRA produces volume unbalances of the LA cylinder chambers which causes different pressure bulid-up dynamics but its effect is negligible. The acceleration disturbances can also generate a severe error for the case of large inertia of the moving element associated to high accelerations.

If the required performance of the load control system is very demanding as for maximum force and frequency response, hydraulic technology allows to meet the requirements utilizing commercially available special components. In order to outilne the rationale for the control strategy developed for the TRA force control system, the system shown in figure 2 can be linearized, considering the load actuator at mid stroke and with small command on the servovalve operating with mean value zero, and analyzed in the frequency domain applying the Laplace transform. By following this approach, the block diagram shown in figure 8 is obtained.

Figure 8 shows how the servovalve and the load cell are modeled as second order systems. As a first order approximation, the dynamics of the servovalve and load cell are neglected and it is possible to write the equation describing the relationship between the force output to the servovalve command *V* and the load actuator velocity established by the TRA:

$$F_C = \frac{K_1 V}{\tau s + 1} - \frac{K_2 + ms + \tau m s^2}{\tau s + 1}\dot{x}_{LA} \tag{5}$$

Where:

$$K_1 = \frac{G_Q A}{k_L + G_Q/G_P} \tag{6}$$

$$K_2 = \frac{A^2}{k_L + G_Q \,/\, G_P} \tag{7}$$

$$\tau = \frac{C}{2\left(k_L + G_Q \,/\, G_P\right)} \tag{8}$$

For a standard PID controller the transfer function $\mathbf{G_{C(s)}}$ is:

$$G_C(s) = K_P + \frac{K_I}{s} + K_D s \tag{9}$$

Equation 9 can be used to calculate the servovalve set point:

$$V = \left(K_P + \frac{K_I}{s} + K_D s\right)(F - F_C) \tag{10}$$

Substituting this expression of V into Equation 5 and disregarding the derivative term (mostly affect the stability without improving the system accuracy), the expression of the actual force F_C developed on the TRA is derived:

$$F_C = \frac{\left(1 + \frac{K_P}{K_I}s\right)F - \frac{s\dot{x}_{LA}}{K_1 K_I}(K_2 + ms + \tau m s^2)}{\frac{\tau}{K_1 K_I}s^2 + \frac{s}{K_1 K_I} + \frac{sK_P}{K_I} + 1} \tag{11}$$

Multiplying numerator and denominator by K_I/s the following equation is obtained:

$$F_C = \frac{F\left(K_P + \frac{K_I}{s}\right) - \frac{\dot{x}_{LA}}{K_1}(K_2 + ms + \tau m s^2)}{\frac{\tau}{K_1}s + \frac{1}{K_1}(1 + K_I K_P) + \frac{K_I}{s}} \tag{12}$$

This equation clearly shows that when the actuator is subjected to a constant velocity disturbances the integrator will eventually cancels out the error, with the settling time being inversely proportional to the integrator gain. However, it is not possible to increase arbitrarily its value in order to maintain and adequate stability margin and also because integrator force controls are subjected to limit cycle oscillations [7], [8]. The reduction of the effects of the disturbances must then be obtained acting on other system parameters. The force error F_D created by the velocity is:

$$F_D = \frac{\frac{\dot{x}_{LA}}{K_1}(K_2 + ms + \tau m s^2)}{\frac{\tau}{K_1}s + \frac{1}{K_1}(1 + K_I K_P) + \frac{K_I}{s}} \tag{13}$$

and replacing the terms K_1, K_2 and τ with their expressions Eq. 8, 9, 10, the following relationship is obtained:

$$F_D = \frac{\left(\frac{A^2}{k_L + G_Q / G_P} + ms + \frac{C}{2(k_L + G_Q / G_P)}ms^2\right)\dot{x}_{LA}}{\frac{C}{2(k_L + G_Q / G_P)}s + K_I K_P + \frac{K_I}{\frac{G_Q A}{k_L + G_Q/G_P}s} + 1} \tag{14}$$

Looking at this expression, it is possible to note that in order to minimize the disturbance effects of the LA rod speed the flow coefficient of the orifice, k_L, and the ratio $G_Q/G_P = G_{PQ}$, flow-pressure gain of the servovalve should be maximized. The flow-pressure gain of the servovalve can be increased either by increasing the supply pressure or by reducing the differential pressure between the cylinder chambers. Increasing the orifice diameter is a simple solution and it is common industrial practice even if requires larger servovalves and pumps. This disturbances compensation is a passive compensation in contrast to more complex strategy based on an active compensation which acts on the servovalve command.

6. Active compensation of disturbances

The parallel use of passive and active disturbances compensation strategies allows to reduce the energy loss due to the flow through the bypass orifice while still maintaining a good disturbances rejection. This is obtained by injecting appropriate corrective commands to the servovalve in order to compensate for the rate of change of volume in the loading actuators chambers due to the actuator load and acceleration.

Analyzing analytically the active compensation problem it is possible to determine that in order to obtain a theoretically perfect speed disturbances rejection a signal proportional to the acceleration must be used. Because direct accelerometric measurement on the rig proved to be a critical issue, the acceleration was numerically calculated from the speed feedback signal. However, the direct calculation of the acceleration from the speed feedback cannot be directly used because when the TRA is loaded it deflects and this deformation is sensed by the measurement chain. The effect of such phenomenon is visible in figure 9 showing the results of simulations representing the speed F/B of the unloaded TRA (upper graph) and the superposition of the displacement speed, harmonic load, and commanded action (lower graph).

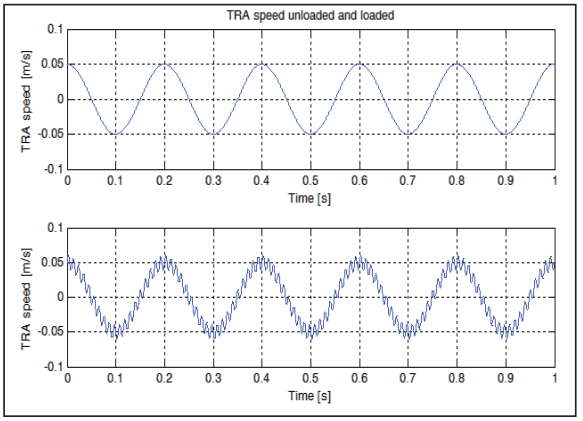

Fig. 9. Effect of harmonic load on the TRA speed F/B

In order to compensate only kinematic disturbs deriving from the TRA commanded actuation the signal must be filtered efficiently minimizing the phase lag. Furthermore, because the loading cycles occur at high frequency, the numerically calculated acceleration signal must be conditioned with a digital filter path in the control system. The series of digital filters is made up by a lead compensator, a low order low pass filter and a variable frequency notch filter centered on the load frequency fist harmonic which is known to the controller since it's user defined. The overall topology of the controller is shown in figure 10:

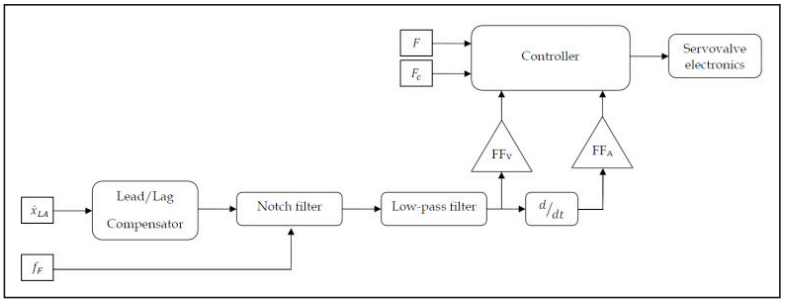

Fig. 10. Force control law diagram

The control loop is closed using the force feedback signal and, to maximize disturb rejection while ensure stability, the active compensation branch generates data used in the control action. Since the rig is used also to reproduce non-harmonic loads the controller is provided with the capability of excluding branches and reconfigure itself in order to maintain the setpoint tracking in such cases.

The frequency response of the complete filtering branch for the specific case of an harmonic load with frequency of 40 Hz is reported as reference:

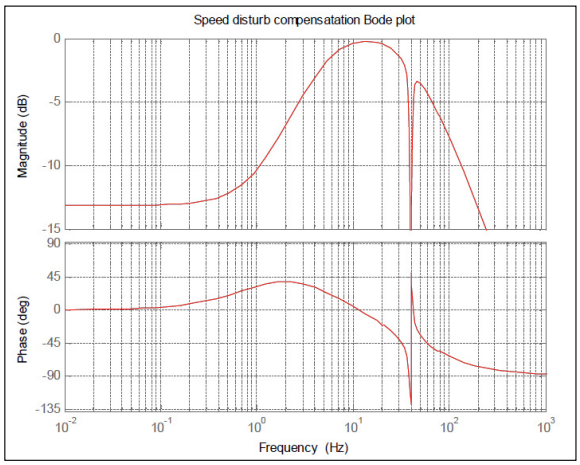

Fig. 11. Bode plot of the velocity filtering branch

The diagram of figure 11 shows a large signal attenuation at low frequency, which implies a little effect of this filter in the low frequency range. This is not a concern, however, because the disturbances at low frequency are well compensated by the standard PID control as well as the by the bypass orifice. On the other hand, at higher frequency the phase lead coupled with the low attenuation of the velocity signal permits a good compensation of the disturbances. The velocity signal, now deprived from the high frequency harmonics, is then differentiated and used for the compensation. In order to compensate also for the acceleration disturbances, the numerically computed derivative signal should be differentiated again. However, since the signal is originated by measurements affected by noise, such operation would generate a too noisy reference unsuitable for the compensation. By exploiting the relationships between time derivatives of a harmonic signal it is possible to estimate the jerk using the acquired velocity values. The filtered velocity and its time derivative are used in parallel when summed to the servovalve command; the two data series are in quadrature, and acting on their gains FF_V and FF_A it is possible to obtain the desired compensation.

Finally it must be underlined that the active compensation branch is fully tunable and its parameters had been chosen in order to maximize its effect at the highest frequency the TRA was able to operate without significant attenuation because, for the specific case, in those regions the actuators was operating at maximum speed under the specified test cases.

7. Conclusive remarks

The topology of the controller and its associated compensator has been defined following a model based approach. Having the system been operational before the control synthesis began allowed to validate experimentally the model of the individual components, when the output of a given subsystem was readily measurable, and of the entire force control rig. Experimental campaigns targeted at the parameter identification allowed to validate the model for disturbed and undisturbed operating conditions, and were instrumental to identify the correct control gains and time constants.

For the main control branch the chosen topology is the standard PID with a clamping anti windup saturation; a feed forward compensation of the time derivative of the force command provided a boost allowing a reduction of the force error at high frequencies, while the kinematic disturbances compensator limited the disturbances effects [9].

Figure 12 presents the experimental frequency response of the test rig operating at different set point amplitudes, this diagram was obtained after the final loop gains tuning. The test campaign showed a peak amplification of the force set equal to +3.6 dB at 35 Hz

and a maximum attenuation of -2.0 dB at 85 Hz; these results met them rig requirements both in terms of set point attenuation and stability margin.

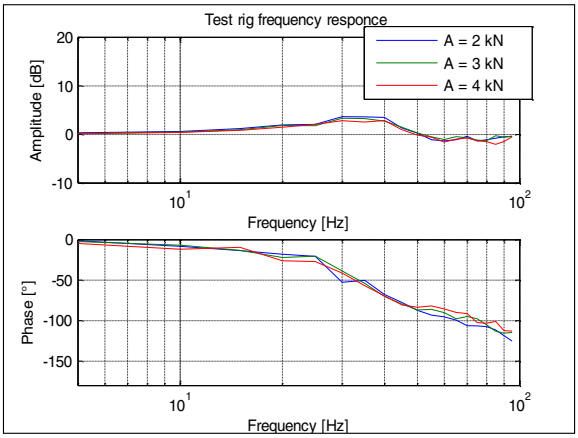

Fig. 12. Experimental frequency response

Acknowledgments

The authors wish to thank UTC Aerospace Systems Italy for the support received during the work that led to this publication.

References

[1] Jacazio, G., and Balossini, G., (2009). "A Mechatronic Active Force Control System for Real Time Test Loading of an Aircraft Landing Gear". In *Proceedings of the ASME 2009 International Design Engineering Technical Conferences & Computers and Information in Engineering Conference* IDETC/CIE 2009, San Diego, August 30-September 2.

[2] Jacazio, G., and Balossini, G., (2007). "Real-time Loading Actuator Control for an Advanced Aerospace Test Rig". In *Proceedings of the Institution of Mechanical Engineers, Part I: Journal of Systems and Control Engineering 2009*.

[3] Jacazio, G., and Balossini, G., (2008). "The Iron Bird for M346 Advanced Trainer". In *SAE A6 Meeting on Aerospace Fluid Power and Actuation Systems, Portland, USA, October 13-16.*

[4] J. A. Ferreira, F. Gomes de Almeida, M. R. Quintas, (2002)."Semi-empirical model for a hydraulic servo-solenoid valve" *Proceedings of the Institution of Mechanical Engineers, Part I: Journal of Systems and Control Engineering May 1, 2002 vol. 216 no. 3 237-248.*

[5] D. C. Pountney, W. Weston. M. R. Baineghbal, (1989)."A numerical study of turbulent flow characteristic of Servo-Valve orifices" *Proceedings of the Institution of Mechanical Engineers, Part A: Journal of Power and Energy May 1989 vol. 203 no. 2 139-147*

[6] Karam, W., and Mare, J.-C., (2007). "The Performance of Force Controlled Electromechanical Actuator Around Null Speed". In *Proceedings of Power Transmission and Motion Control Symposium PTMC 2007, Bath, UK, September 12-14*

[7] Jean-Charles Mare, (2006) "Dynamic loading systems for ground testing of high speed aerospace actuators", *Aircraft Engineering and Aerospace Technology, Vol. 78 Iss: 4, pp.275 – 282.*

[8] Di Rito, G., (2007). "Experimental Implementation of a Motion- Compensated Force Control in a Hydraulic Workbench for Flight Actuators". In *Proceedings of the Recent Advances in Aerospace Actuation Systems and Components 2007 Conference, Toulouse, France, June 13-15, pp. 51–57.*

[9] Mare, J.-C., and Karam, W. (2008) "Force Control of a Roller-Screw Electro-Mechanical Actuator for Dynamic Loading of Aerospace Actuators". In *Proceedings Bath/ASME Symposium on Fluid Power and Motion Control, Bath, UK, September 10-12 2008.*